Antiprotonic Helium – An Exotic Hydrogenic Atom

Toshimitsu Yamazaki

RI Beam Science Laboratory, RIKEN, 2-1 Hirosawa, Wako-shi, Saitama-ken, 351-0198, Japan. E-mail: yamazaki@nucl.phys.s.u-tokyo.ac.jp

Abstract. The *antiprotonic helium*, $\bar{p}e^-He^{2+}$ ($=\bar{p}He^+$), is a peculiar metastable atom, interfacing between matter and antimatter. A series of metastable states are composed of the He nucleus, one electron in the ground 1s configuration and one antiproton orbiting with large quantum numbers (n, l), where $n \sim l \sim \sqrt{M^*_{\bar{p}}/m_e} \sim 38$. They possess a dual character as an exotic atom and an exotic diatomic molecule, and is often called *antiprotonic helium atom-molecule*, or for short, *atomcule*. From the chemical physics point of view the $\bar{p}He^+$ may be regarded as an exotic neutral hydrogen atom with a composite "pseudo proton" with various effective charges, binding energies and spatial distributions. Since its discovery in 1991 at KEK comprehensive experimental studies have been carried out at CERN. In particular, the laser resonance spectroscopy of $\bar{p}He^+$ has yielded the following results. 1) Precise determination of the transition energies to the precision of ppm. When compared with advanced theoretical predictions of the binding energies of this Coulomb 3-body system including the relativistic effects and QED corrections, the mass and charge of $\bar{p}$ have been determined with ppm precision. 2) Hyperfine structure of $\bar{p}He^+$ due to the coupling of the electron spin with the large orbital magnetic moment of $\bar{p}$ has been revealed experimentally. 3) The dependence of the lifetimes of the individual (n, l) states of $\bar{p}He^+$ on the He medium density, foreign atoms and molecules has been studied with the laser tagging method.

1 Introduction

Longevity of any particle system or atom is an essential clue for high-precision experiments. Furthermore, it provides an extended time range during which time-dependent dynamical processes can be studied in real time. In the field of exotic atoms, namely, bound systems involving negative hadrons such as pion (π^-) and kaon (K^-), no long-lived state was expected, since the negative hadrons are subject to prompt nuclear absorption after their atomic capture in matter. The muon and muonium are exceptional because they have no strong interactions, and their lifetime of 2.2 μs has consequently facilitated muon spin rotation spectroscopy (μSR) as well as laser/microwave spectroscopy. The antiproton is believed to annihilate immediately in matter due to the strong interation. Thus, modern methods as applied for muon and muonium had not been conceived for antiprotons before the discovery of anomalous $\bar{p}$ longevity in liquid helium in 1991 [1] and in other phases of helium [2].

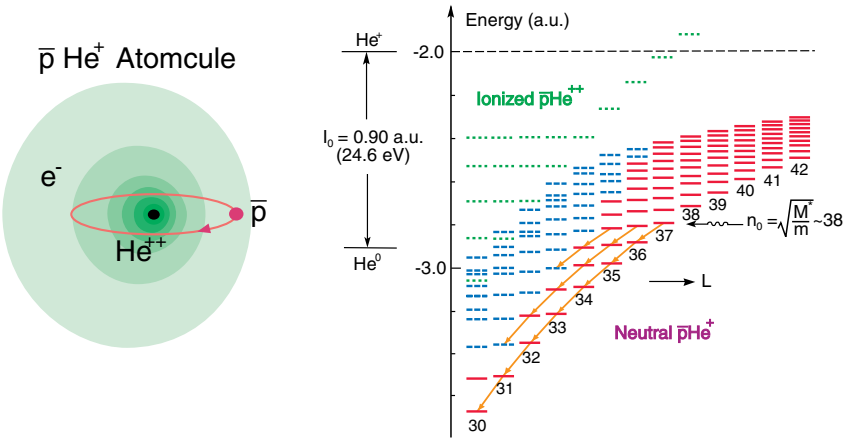

Fig. 1. (Left) The structure of the $\bar{\mathrm{p}}\mathrm{He}^+$ atomcule, where the $\bar{\mathrm{p}}$ with large-(n,l) quantum numbers circulates in a localized orbit around the He^{2+} nucleus, while the electron occupies the distributed 1s state. (Right) The level scheme of large-(n,l) states of the $\bar{\mathrm{p}}\mathrm{He}^+$ atomcule. The solid bars indicate radiation-dominated metastable states, while the broken lines are for Auger-dominated short-lived states. The ionized $\bar{\mathrm{p}}\mathrm{He}^{++}$ states are also shown by dotted lines. From Ref. [2]

The cause of the $\bar{\mathrm{p}}$ longevity is the formation of various metastable states of $\mathrm{e}^-\bar{\mathrm{p}}\mathrm{He}^{2+}$ $(=\bar{\mathrm{p}}\mathrm{He}^+)$ in helium media. They are collectively called *Antiprotonic Helium*.

- **Formation**: When an $\bar{\mathrm{p}}$ slows down in He, its kinetic energy eventually falls below the He ionization threshold ($I_0 = 24.6$ eV), at which point it replaces one of the electrons in a He atom to form $\bar{\mathrm{p}}\mathrm{He}^+$. The antiprotonic helium atom thus formed with an initial kinetic energy around 5 eV reaches thermal equilibrium within nanosecond without suffering destruction.
- **Structure**: Whereas the remaining e^- stays in the 1s ground orbital, the captured $\bar{\mathrm{p}}$ occupies a large-(n,l) state: $n \sim n_0 = \sqrt{M^*/m_e} \sim 38$, where M^* is the reduced mass of the $\bar{\mathrm{p}}$-He system. The angular momentum l which is brought by the captured $\bar{\mathrm{p}}$ can be as much as that of the circular state, $l \sim n-1$. As shown in Fig. 1, the $\bar{\mathrm{p}}$ is orbiting in a classical trajectory, while the e^- is distributed quantum mechanically.
- **Stability and Decay**: Metastability of $\bar{\mathrm{p}}\mathrm{He}^+$ occurs in a limited zone of (n,l) around $(38,37)$ due to the following three reasons jointly, as asserted by Condo [3] and Russell [4] in earlier days before the discovery of the $\bar{\mathrm{p}}$ longevity.
  a *Suppressed Stark decay*: The neutral system $\mathrm{e}^-\bar{\mathrm{p}}\mathrm{He}^{2+}$ involving one electron is protected from intruding He atoms by the Pauli exclusion. Furthermore, it is resistant to collisional Stark effects in helium medium, because the presence of e^- removes the l degeneracy for the same n, sharply reducing the corresponding Stark mixing amplitudes.

b *Suppressed Auger decay*: Because of the large ionization energy ($\sim$ 25 eV) compared with the $n \to n-1$ level spacings (typically, $\sim$ 2 eV), the Auger process from near-circular states ($l \sim n-1$) is associated with a large angular momentum jump (larger than 3 $\hbar$), and thus is highly hindered.

c *Slow radiative decay*: The remaining decay process is a slow radiative decay because of the small level spacings (around 2 eV) and of the retardation mechanism due to the e^--$\bar{p}$ correlation. The level scheme is shown in Fig. 1. The main cascade is subject to *Propensity Rule*:

$$\Delta v = \Delta(n-l-1) = 0, \text{ or : } \Delta n = \Delta l = \pm 1, \tag{1}$$

because of the well localized $\bar{p}$ orbits. The other dipole transitions are highly suppressed. The typical level lifetime is 1.5 μs [5,6]. The transition $(n,l) \to (n-1, l-1)$ is of normal strength and is often called "favoured transition", while the other transitions are hindered due to the small overlap of the wavefunctions, and are called "unfavoured transitions". They are not spontaneous transitions, but can be stimulated by laser resonances.

2 Unique Facets of Antiprotonic Helium

Antiprotonic Helium has many interesting facets because of its unique three-body character involving one $\bar{p}$ and thus provides playgrounds of physics and chemistry.

- **Primordial exotic atom:** The metastable states are located in the "primordial" zone ($n \sim n_0 = \sqrt{M^*/m_e}$), where the exotic particle and the atomic electron coexist in the same spatial region. With the exception of antiprotonic helium, the primordial zone of exotic atoms has never been identified and remains an untouched object of investigation.
- **Exotic ground-state hydrogen atom:** Antiprotonic Helium is an exotic kind of hydrogen atom like positronium (Ps) and muonium (Mu), if we regard the $[\bar{p}He^{2+}]_{(n,l)}$ as a "proton" by which the electron is bound. The "proton" in this case possesses various "excited states" (n,l), and the effective charge and binding energy of the electron are more like those of helium atom and are dependent on the antiprotonic quantum numbers (n,l). Thus, Antiprotonic Helium can be an interesting subject of chemical physics.
- **Atomic core polarization: e^--$\bar{p}$ correlation:** Yamazaki and Ohtsuki [5] emphasized the important role of a special type of configuration mixing which contributes to a substantial reduction of the radiative transition rate. This effect is essentially the same as in the nuclear core polarization phenomena, where low energy transition moments are affected by the presence of high excitation mode (giant resonances). In the present case, the low energy E1 transitions ($\sim$ 2 eV) are retarded by a factor of 3 by the existence of the hard electronic excitation ($\sim$ 20 eV).

- **Exotic diatomic molecule:** The two-body exotic atom consisting of a nucleus and a heavy exotic particle X^- is described by a potential $U(r)$ that consists of an attractive long-range Coulomb potential and an repulsive short-range centrifugal potential. The potential $U(r)$ resembles a Morse potential, when the exotic particle has a sufficiently large angular momentum (hence large n). The system thus looks rather like a molecule, to which rotational (J) and vibrational (v) quantum numbers may be uniquely assigned as

$$rotation - vibration \quad J = l,\ v = n - l - 1. \tag{2}$$

  Namely, the circular orbit ($l = n - 1$), which is a rotating state with a nodeless radial wavefunction, corresponds to a vibrational quantum number $v = 0$, and the next-to-circular single-node state ($l = n - 2$) corresponds to $v = 1, \ldots$. This theoretical possibility of large-l circular orbits behaving like bound states in a Morse potential seems to have no other natural manifestation than in the present case of metastable exotic helium. This situation is presented in Fig. 2, where the potential as well as the wavefunctions are shown.
  The $\bar{p}$ and He^{2+} are thus regarded as two atomic centers in a diatomic molecule. Because of the dual character as an exotic atom and an exotic molecule Antiprotonic Helium is often called *antiprotonic helium atom-molecule*, or for short, *atomcule*. Since the 1s electron motion, coupled to a large-(n, l) $\bar{p}$ orbital, is faster by a factor of 40 than the $\bar{p}$ motion, the three-body system $\bar{p}He^+$ is solved by using the Born-Oppenheimer approximation, as fully discussed by Shimamura [6].
- **Unique interface between matter and antimatter:** Whereas particles and antiparticles cannot coexist stably, Antiprotonic Helium is an exceptional case, where an intruder antiparticle ($\bar{p}$) coexists with the normal matter (helium medium) for microseconds. Here, the property of the orbiting $\bar{p}$ (charge, mass, magnetic moment and other QED characteristics) can be probed. It is an interesting irony that the property of the proton cannot always be studied so precisely, because there is no atomic system in which a proton is orbiting.

3 Advanced Theories

As of 1994 the configuration interaction theory of Ohtsuki [5] and the molecular theory of Shimamura [6] played important guiding roles for experimentalists in their study of the peculiar phenomena of the $\bar{p}$ longevity. After 1995 more sophisticated theoretical methods have been developed. These overcome the intrinsic limitation of treating the $\bar{p}He^+$ system in adiabatic approximation by covering the molecular aspects and the configuration interaction aspects equally well.

- **Molecular expansion variational method:** Korobov [7] developed a variational method using the molecular-type basis functions involving excited

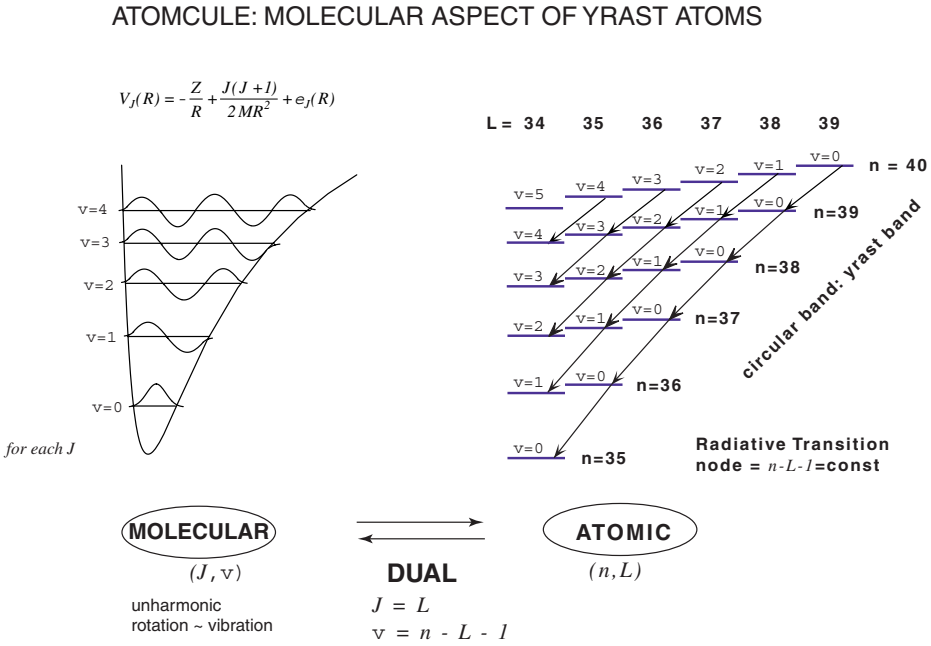

Fig. 2. Atomic and molecular views of Antiprotonic Helium. The large (n, l) states in the atomic yrast region in the atomic model are also assigned as the molecular states of corresponding rotational and vibrational quantum numbers $(J, v) = (l, n - l - 1)$ in the one-dimensional potential for each J. The radiative transitions with $\Delta v = 0$, as shown by arrows, are favoured because of the maximum overlapping of the radial densities. In this sense, the atomcule system has a dual character by itself

electronic configutations. He showed that the binding energies converge to a precision of 14 digits when the number of the basis functions is 2300. This assures a precision of 13 digits for transition energies between metastable states.

- **Coupled-rearrangement-channel variational method:** Kino, Kamimura and Kudo [8] developed a variational method employing three types of coupling schemes among $\bar{\mathrm{p}}$, e^- and He^{2+}, which also combined the molecular base and the electronic configurations. Their calculational precision is as high as Korobov's.
- **Finite-element numerical calculation method:** Elander and Yarevsky [9] solved the three-body system by employing the finite-element numerical method. The precision achieved in this method is impressively high.

4 Laser Spectroscopy of Antiprotonic Helium

Laser spectroscopy of $\bar{\mathrm{p}}\mathrm{He}^+$ was established according to the proposal of Morita *et al.* [10], which is to apply a pulsed laser tuned to a transition between a

metastable and a short-lived state. Such a "metastable-short-lived" pair exists at the end of each metastable cascade of a quantum number $v = n - l - 1$ and also between (n, l) and $(n+1, l-1)$. The transition dipole moments for favoured $((n, l) \leftrightarrow (n-1, l-1))$ and unfavoured $((n, l) \leftrightarrow (n+1, l-1))$ transitions are of the following orders:

$$\textit{Favoured}: \quad \mu \sim 0.2 - 0.3 \text{ Debye}; \tag{3}$$

$$\textit{Unfavoured}: \quad \mu \sim 0.02 - 0.03 \text{ Debye}. \tag{4}$$

The wavelengths of the laser resonances tend to form clusters, because the energy spacings, $E(n, l) - E(n-1, l-1)$, depend nearly linearly on the value n, but only slightly on l.

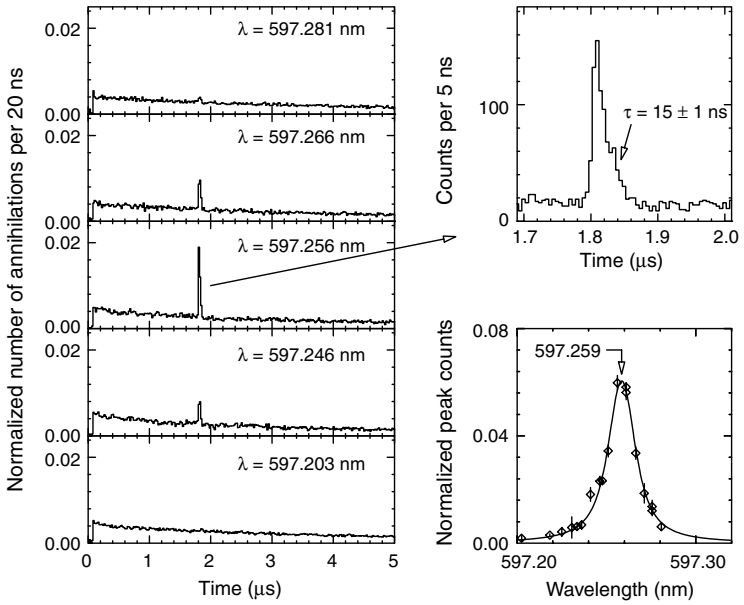

Fig. 3. First successful observation of laser resonance of antiprotonic helium, now attributed to the $(n, l) = (39, 35) \rightarrow (38, 34)$ transition. (Left) Observed time spectra of delayed annihilation of antiprotons with laser irradiation of various vacuum wavelengths near 597.2nm. Spikes due to forced annihilation through the resonance transitions are seen. (Upper right) Enlarged time profile of the resonance spike. (Lower right) Normalized peak count versus vacuum wavelength in the resonance region. From Morita *et al.* [11]

The first successful experiment of laser resonances was on the 597 nm transition $(39, 35) \rightarrow (38, 34)$ [11,12] (see Fig. 3), and the second search was carried out for the 470 nm $(37, 34) \rightarrow (36, 33)$ transition [13]. These experiments on

the $\Delta v = 0$ transitions proved the structure of $\bar{p}He^+$ as predicted [5,6] and revealed for the first time that the primordial states of exotic atoms with quantum numbers $n \sim \sqrt{M^*/m_e}$ are indeed populated. The initial population of various metastable states as studied by the laser technique gave important data to the theoretical prediction by Korenman [14].

Subsequently, search for unfavoured resonances of $\Delta v = 2$ $(n, l) \rightarrow (n + 1, l - 1)$ transitions was carried out [15] with the following motivations. They were expected to yield qualitatively different type of information on the binding energies of $\bar{p}He^+$. As $\Delta v = 0$ transitions alone do not yield energy differences between bands of differing v, information on interband $\Delta v = 2$ transitions is vitally important for a stringent test of theory. Later, the $\Delta v = 2$ interband character was found to be essential in finding a hyperfine structure effect [16].

5 Precise Determination of Transition Energies

As of 1994 the agreement between experiment and theory in the observed transition wavelengths was of the order of 1000 ppm. Then, a new theory of Korobov [7] came in. Fig. 4 shows comparison between experiment and theory. Although Korobov's non-relativistic theory showed a dramatical improvement over the earlier theories, it revealed a systematic discrepancy of the order of 50-100 ppm. This urged Korobov and Bakalov to take into account relativistic corrections [17]. The relativistic corrections are systematically about 50 ppm for the $\Delta v = 0$ transitions and about 100 ppm for the $\Delta v = 2$ transitions, accounting for the experimental results very well.

During the course of laser resonance experiments it was noticed that the central wavelengths shift depending on the helium density. Thus, the resonance line shapes at various target gas conditions were measured precisely with a reduced laser bandwidth and an improved wavelength calibration [18]. Figure 5 shows resonance profiles taken for the 597.26 nm line at different pressures ranging from 530 mb to 8.0 bar at temperatures of 5.8–6.3 K. The results are summarized in Table 2.

After the corrections for the pressure shifts Torii *et al.* [18] obtained wavelengths in vacuum, which revealed a small discrepancies of several ppm, as shown in Fig. 6. The theoretical values are further corrected for QED effects [9,19,20], yielding excellent agreements to ppm precision. Various QED corrections calculated by Korobov [21] are itemized in Table 1.

The excellent agreement between experiment and theory is used to deduce a constraint on the assumed mass $M_{\overline{p}}$ and charge $Q_{\overline{p}}$ of antiproton. While the cyclotron frequency of $\bar{p}$ measured by Gabrielse *et al.* [22] sets a severe constraint on the ratio $M_{\overline{p}}/Q_{\overline{p}}$, the antiprotonic helium gives a constrant on the "$\bar{p}$ Rydberg constant" $M_{\overline{p}}Q_{\overline{p}}^2$ *a la* Hughes and Deutch [23]. Combining these two physical quantities we obtain $M_{\overline{p}}$ and $Q_{\overline{p}}$ independently. The constraints thus obtained are shown in Fig. 7.

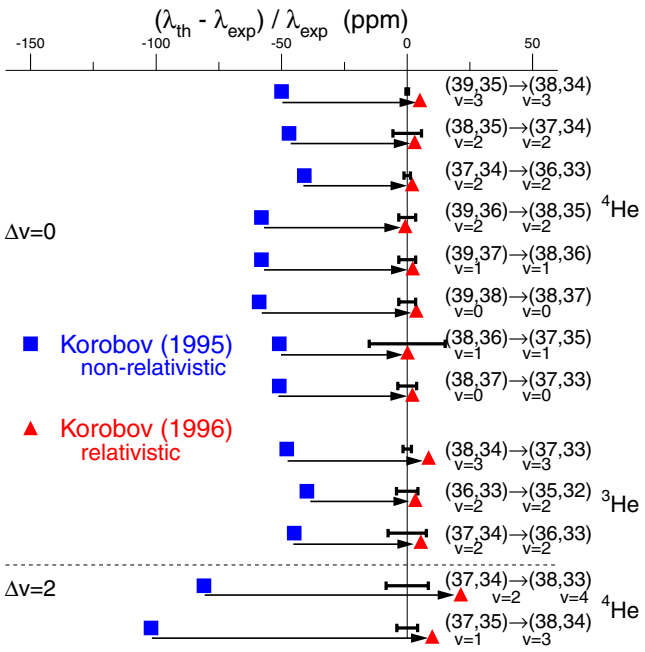

Fig. 4. Comparison of the experimental wavelengths of various transitions with Korobov predictions (closed squares without [7] and closed triangles with [17] relativistic corrections). The upper part is for $\Delta v = \Delta(n - l - 1) = 0$ intraband transitions and the lower part is for $\Delta v = 2$ interband transitions. The error bars are the experimental ones

6 Chemical Physics Aspects

The metastablity of antiprotonic helium is known to be affected when foreign atoms and molecules are added to the helium media, as revealed from delayed annihilation time spectra (DATS) in the early stage [2,24,25]. However, DATS alone is a macroscopic quantity in which all the microscopic informations cannot be differentiated. Laser resonance techniques have made it possible to investigate microscopically the (n, l)-dependent lifetime shortening effects on the surrounding physico-chemical conditions of antiprotonic helium.

6.1 State Dependent Lifetime Shortening

The lifetimes of the metastable states $(n, l) = (39, 35)$ and $(37, 34)$, which are the parent states of the 597.26-nm and 470.72-nm resonances, respectively, demonstrate interesting density effects [26]. The intensity of the 597.26 nm resonance

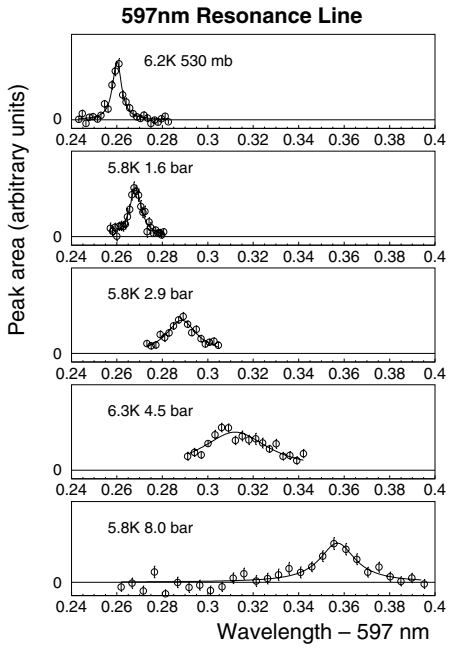

Fig. 5. Resonance profiles of the 597.26-nm line showing red-shifts of the center with helium density. The linear scale for the y axes is not the same for different target conditions. From Torii *et al.* [18]

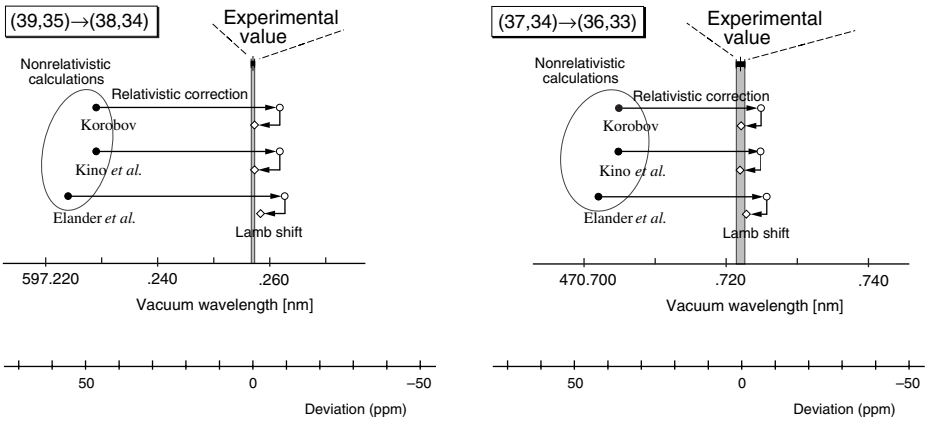

Fig. 6. The experimental values of the vacuum wavelengths for transitions (39,35)→(38,34) and (37,34)→(36,33) are compared with recent theoretical values [,19,20], which agree within precisions of a few ppm when the relativistic corrections and the Lamb shift are taken into account. From Torii *et al.* [18]

Table 1. Summary of various contributions on the transition energy of the $(39, 35) \rightarrow (38, 34)$ of $\bar{\mathrm{p}}^4\mathrm{He}^+$. From [21]. The experimental value is [18]

Term	Notation	Energy (in GHz)
Non-relativistic energy	E_{NR}	501972.374(21)
Relativistic correction	ΔE_{rc}	-27.556
Relativistic correction (QED)	ΔE_{rc-qed}	0.233
Self energy	ΔE_{se}	3.815
Vacuum polarization	ΔE_{vp}	-0.123
Relativistic Recoil	ΔE_{RMC}	0.037
Relativistic Recoil	ΔE_{ret}	-0.035
Two-loop corrections	ΔE_{2-loop}	0.001
Nuclear finite size	ΔE_{nuc}	0.002
α^4 correction	ΔE_{α^4}	-0.003(3)
Total theoretical	E_{tot}	501948.746(21)
Experimental	E_{exp}	501948.8(3)

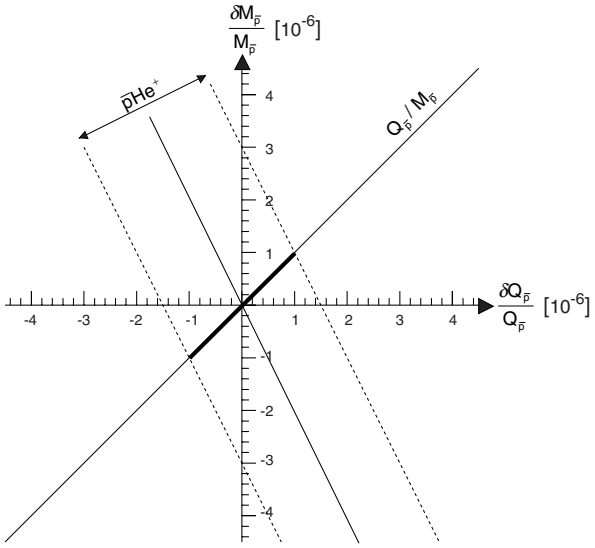

Fig. 7. Two-dimensional constraint on $\Delta M_{\overline{p}}/M_{\overline{p}} = (M_{\overline{p}} - M_p)/M_{\overline{p}}$ and $\Delta Q_{\overline{p}}/Q_{\overline{p}} = (Q_{\overline{p}} - Q_p)/Q_{\overline{p}}$ obtained from the cyclotron frequency of $\overline{p}$ [22] and from the present spectroscopic studies of $\bar{\mathrm{p}}\mathrm{He}^+$ [18]

spike measured at densities between 2×10^{20} cm^3 (corresponding to a target condition of 0.2 bar and 6.8 K) and 1.9×10^{22} cm^3 (8.7 bars and 5.8 K) is relatively constant (Fig. 8, left), indicating that the state lifetimes and initial populations of states in the $v = 3$ cascade are unaffected over this density range.

The recovery rate of the time spectrum after the resonance depletion showed the lifetime of the resonance parent state (39,35) was constant at ~ 1.5 μs regardless of density (Fig. 8, left).

In contrast, a drastic density effect was observed for the 470-nm resonance. The depletion-recovery time spectrum (Fig. 8, right) shows that as the density increases from $\rho = 1.2 \times 10^{20}$ to 3×10^{21} cm^{-3}, the state lifetime decreases from $\tau = 1.2$ to 0.1 μs and levels off at higher densities.

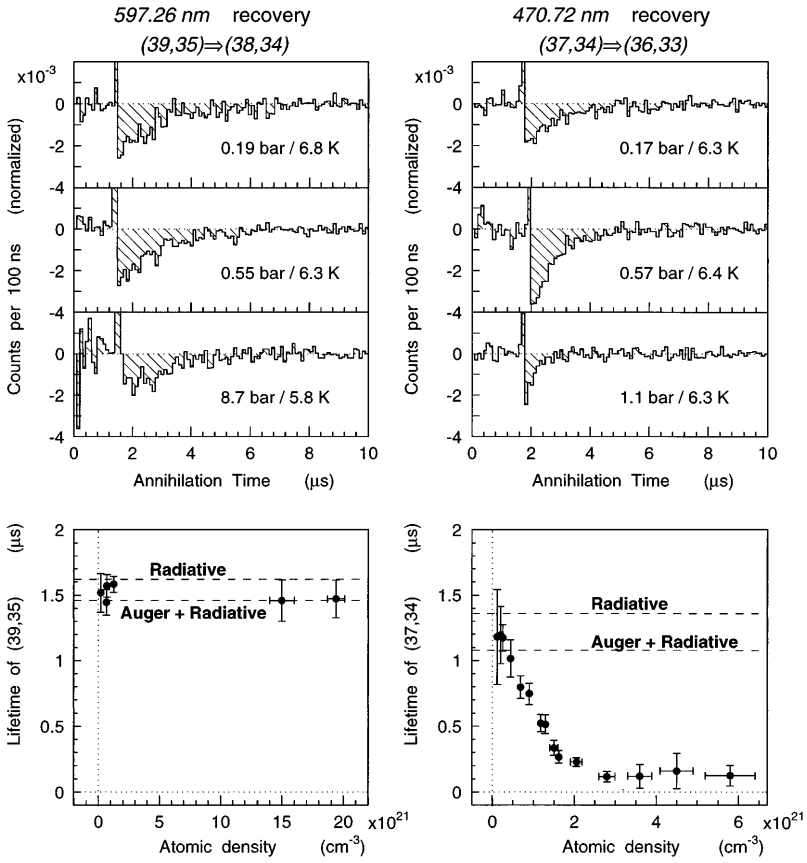

Fig. 8. Depletion-recovery spectra of the 597.26-nm (left) and 470.72-nm (right) resonances at various target densities. The lifetimes of the radiation-dominated parent states $(n, l) = (39, 35)$ and $(37, 34)$ are plotted as a function of density. The $(37, 34)$ state becomes short lived with increased density, while the higher-lying $(39, 35)$ remains unaffected. Theoretical radiative rates and the sum of radiative and Auger rates are also shown [27]. From Hori *et al.* [26]

The distinct and peculiar state dependence of this particular level lifetime has not yet been understood.

6.2 Pressure Shifts of Resonance Lines

The results of the pressure shift measurements on the two transitions (see Fig. 5) are presented in Table 2. There is a distinct difference between the $(39, 35) \rightarrow (38, 34)$ and $(37, 34) \rightarrow (36, 33)$ transitions. The presence of pressure shifts and broadening in resonance profiles is a well known general phenomenon. The present finding in $\bar{p}He^+$ differs somewhat from usual in that the pressure shift is small (and with a substantial (n, l) dependence), and that the broadening is much smaller than the shift, while in ordinary atoms and molecules $\Delta\Gamma$ is observed to be comparable to $\Delta\nu$.

Recently, this problem was treated by a rigorous quantum chemistry calculation by Bakalov *et al.* [28]. First, the authors calculated *ab initio* the interatomic interaction $V(R, r, \theta)$ between an atomcule $\bar{p}He^-$ and a He atom based on the Born-Oppenheimer approximation. Since the rotational frequency of the $\bar{p}$ (of order of 10^{15} s^{-1}) is much higher than the collision frequency (of order of 10^{12} s^{-1}), the angular dependence is smeared out, and typically, the Van der Waals minimum occurs around $R \sim 5.5$ a.u., and the repulsive barrier starts around $R \sim 5$ a.u. The potential $V(R)$ depends on (n, l), and thus, a small difference $\Delta V(R)$ occurs between an initial state and a final state. It is this difference that causes pressure shifts and broadening in the resonance line.

Bakalov *et al.* treated the trajectories of the helium atom in collision with $\bar{p}He^+$ in a semiclassical way, and calculated the pressure shifts and broadening. They obtained numerical values for a numer of transitions, as presented in Table 2. For the precisely known transitions $(39, 35) \rightarrow (38, 34)$ and $(37, 34) \rightarrow (36, 33)$ their theoretical values with realistic collision trajectories (not the linear approximation) turned out to be in excellent agreement with the experimental values. The theoretical treatment of Bakalov *et al.* was the first quantum chemistry type calculation on the interaction of antiprotonic helium with other atoms and molecules.

6.3 Quenching with H_2 Admixtures

Fig. 9 shows DATS of pure helium and helium with several concentrations of hydrogen in the range of 2 – 1000 ppm [29]. The DATS of pure He at the present condition of 30 K and 1.1 bar (corresponding to a density of 2.6×10^{20} cm^{-3}) exhibits a small initial decaying component (see the inset of Fig. 9), typical for DATS at this density. The characteristic effect on the DATS of adding H_2 molecules is the conversion of some long-lived states to shorter-lived ones. Even with 2 ppm H_2 admixture the DATS reveals the onset of a small (but larger than in the pure He case) fast decaying component. If all the states were

Table 2. Pressure shifts ($\Delta\nu/\rho$) and broadening ($\Delta\Gamma/\rho$) of various transitions in $\bar{p}^4He^+$, obtained experimentally, compared with the predictions of Bakalov *et al.* [28]. In the first two transitions the pressure shifts were precisely determined by Torii *et al.* [18]. The experimental values in the lower part were obtained by ascribing the differences between the observed wavelengths and Korobov's final theoretical values to pressure shifts

Transition	$\Delta\nu/\rho$ (10^{-21} GHz cm^3)		$\Delta\Gamma/\rho$ (10^{-21} GHz cm^3)	
$(n_i, l_i)v_i \rightarrow (n_f, l_f)v_f$	Experiment	Bakalov	Experiment	Bakalov
$(39, 35)3 \rightarrow (38, 34)3$	-4.05 ± 0.07	-3.96	0.30 ± 0.15	0.35
$(37, 34)2 \rightarrow (36, 33)2$	-1.50 ± 0.10	-1.42	< 1.0	0.07

uniformly quenched with the same cross section (as happens for O_2 admixtures [30]) the the DATS would approach a single exponential shape with a decay constant governed by the quenching rate. This is clearly not the case for H_2 admixtures: with increasing H_2 concentration the fast component that appears at low concentrations grows, while the long-lived remainder gradually decreases.

This indicates that the quenching is not a uniform process; some states being destroyed more quickly than others. From the information contained in the DATS alone, however, it would be impossible to draw a unique conclusion about which states are more and which less affected by H_2 admixtures, but the laser tagging method clarified that the upper states are more strongly quenched than the lower states [29,31,32].

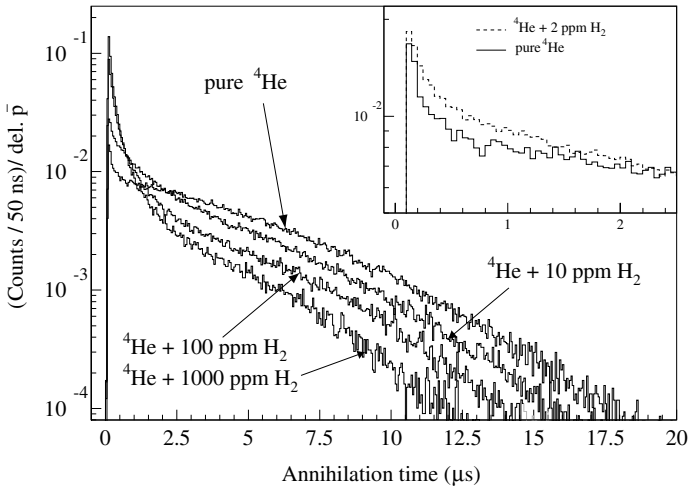

Fig. 9. DATS with various concentrations of H_2 admixtures in helium medium of 1.1 bar at 30 K. The prompt time region is removed in the data taking stage and all the spectra are normalized so as to give the same total delayed fraction. The inset compares the early time region of pure helium and 2 ppm hydrogen admixture. From Ref. [29]

6.4 Hydrogen-Assisted Inverse Resonances and Individual Quenching Rates

If the fact that the upper state (39,35) was found to be destroyed more strongly than the lower state (37,34) is a general tendency, we may be able to quench the metastable states successively from upper to lower states. This expectation was indeed confirmed by inducing laser resonance transitions from lower metastable states to respective upper states [31]. The method is called *Hydrogen-assisted inverse resonances (HAIR)*. The observed transitions are shown in Fig. 10. The HAIR transitions can yield information on the quenching cross sections of both the daughter and parent states of the respective transitions. The lifetime of the parent state can be obtained either from the decay time constant of the peak ($T_1 = \tau$ in this case because of the lack of feeding transitions) or from the depletion recovery. Typically, the lifetime of the parent state is around 600 ns, about 6 times as long as the daughter lifetime. This indicates the interesting and favourable fact that the quenching cross section for the upper state $(n+1, l+1)$ is about 6 times larger than that for the lower state (n, l). The obtained quenching cross sections are shown in Fig. 10 (lower). The cross section has a smooth dependence on (n, l).

Some possible mechanisms for the quenching of $\bar{\mathrm{p}}\mathrm{He}^+$ states were discussed in [29]. First, it is to be noted that the antiprotonic helium resembles a hydrogen-like atom from the physico-chemical point of view, since the $\bar{\mathrm{p}}\mathrm{He}^+$ system has only one electron. The "proton" in this system is a high-lying state $[\bar{\mathrm{p}}\mathrm{He}^{2+}]_{(n,l)}$ with a net charge +1, but an effective charge around 1.6, depending on (n, l). The other view of antiprotonic helium is that it is a kind of diatomic molecule with the two centers $\bar{\mathrm{p}}$ and He^{2+}. One of the plausible processes is *exotic molecule formation*:

$$(\overline{\mathrm{p}}\mathrm{He}^+)_{n,l} + \mathrm{H}_2 \rightarrow [(\overline{\mathrm{p}}\mathrm{He}^+)_{n',l'}\mathrm{H}] + \mathrm{H}\ . \tag{5}$$

This process resembles the $\mathrm{X} + \mathrm{H}_2 \rightarrow \mathrm{XH} + \mathrm{H}$, one of the most fundamental chemical reactions. In the present case, X is a hydrogen-like but with many excited degrees of freedom and effective charges. Since the molecular binding between $\bar{\mathrm{p}}\mathrm{He}^+$ and H is expected to be stronger than the H-H binding due to the larger effective charge of $\bar{\mathrm{p}}\mathrm{He}^+$, the above exotic molecule formation is highly possible. The antiprotonic orbit in the formed molecule will be different from the ones in the atomcule, and the metastability may therefore disappear. Resonant exotic molecules, as seen in muon-catalyzed fusion processes, may also be formed and decay into short-lived channels. Whether such processes can explain the sensitive state dependence or not is however an open question.

7 Hyperfine Structure

So far, we have considered each atomcule state as a single state with quantum numbers (n, l). More precisely speaking, however, since an electron in the 1s orbital is coupled to the antiproton, each state has a hyperfine structure, as is well known for the hydrogen atom. In the present atomcule case, the situation is

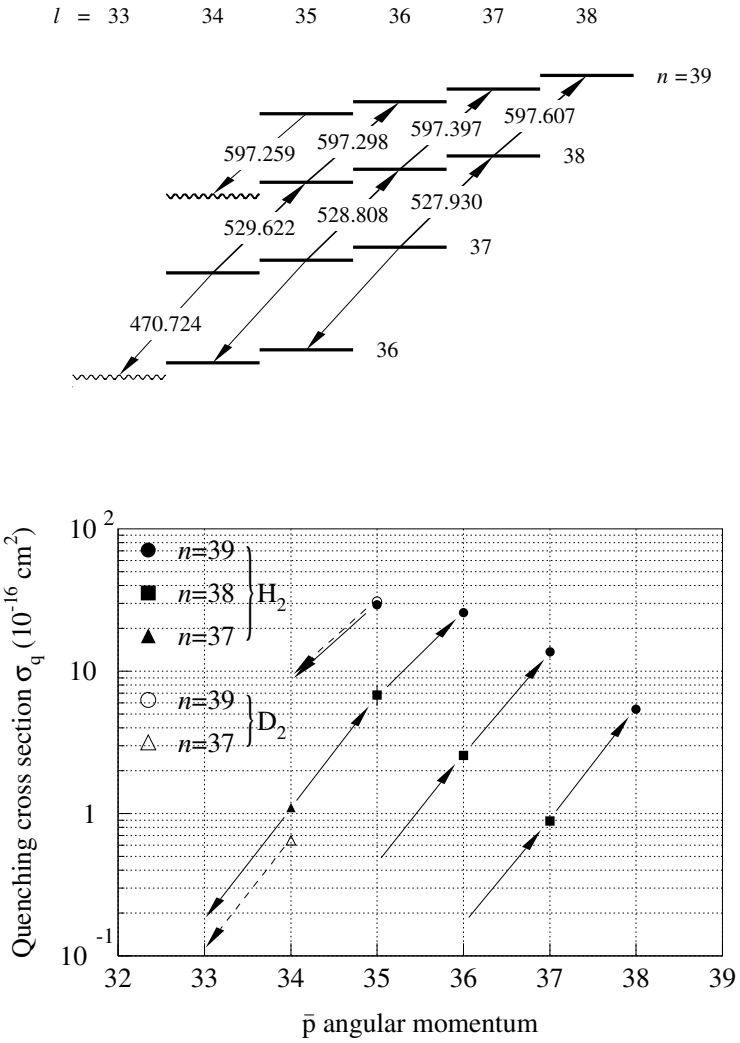

Fig. 10. (Upper) Partial level scheme of $\bar{p}He^+$, summarizing the six transitions between normally metastable states observed by the new HAIR method (bold arrows). Only the vacuum wavelengths for transitions observed until now are shown (in units of nm). (Lower) Dependence of the quenching cross section σ_q by H_2 (full symbols) and D_2 (open symbols) on the quantum numbers n and l. Arrows pointing downwards indicate laser induced transitions between a metastable and a short-lived state, while those pointing upwards represent HAIR transitions between a long-lived lower state and a H_2-induced short-lived upper state. From Ketzer *et al.* [31,32]

more complicated and unique. The most dominant effect must be the coupling of the antiprotonic magnetic moment

$$\boldsymbol{\mu}(\overline{p}) = [g_s(\overline{p})\boldsymbol{s}_{\overline{\boldsymbol{p}}} + g_l(\overline{p})\boldsymbol{l}_{\overline{\boldsymbol{p}}}]\mu_N \tag{6}$$

with the electron spin, because the magnetic moment of e^- is overwhelmingly large. It is interesting to see in eq. 6 that the orbital magnetic moment is much larger than the spin magnetic moment simply because of the large value of $l_{\overline{p}}$. Thus, the coupling of $\boldsymbol{\mu}(\overline{p})$ with the electron spin makes a doublet with quantum numbers

$$\boldsymbol{F} = \boldsymbol{L} + \boldsymbol{S_e}, \quad F_{+/-} = L \pm 1/2. \tag{7}$$

Contrary to the case of hydrogen/muonium ground states, the F_- state lies higher than the F_+ state because in the present case the "nuclear moment" is negative because of the negatively charged $\bar{p}$.

In the atomcule case, we have an additional effect, that is, the coupling of the $\bar{p}$ spin ($\boldsymbol{S_p}$) with the orbital angular momentum of $\bar{p}$ ($\boldsymbol{l_p}$). In a $\bar{p}$-nucleus two-body system this is the spin-orbit coupling, causing a fine-structure doublet. The spin-orbit (ls) splitting for a two-body case is given [34] as

$$\Delta E_{ls}(n,l) = (1+2\kappa)\frac{Mc^2}{2}\frac{(Z\alpha)^4}{n^3 l(l+1)}, \tag{8}$$

where κ is a parameter for the anomalous magnetic moment of $\bar{p}$, as defined by

$$\mu_{\overline{p}} = -(1+\kappa)\mu_N. \tag{9}$$

The well known parameter for proton is $\kappa = 2.79 - 1 = 1.79$. Kreissl *et al.* [35] determined the magnetic moment of $\bar{p}$ as -2.8005(90) μ_N from the measurement of an $n = 11 - 10$ antiprotonic X-ray transition in ^{208}Pb.

As formulated by Bakalov and Korobov [33], each state of (n, L) is split into doublet states (HFS) by the coupling of the electron spin (S_e) and the $\bar{p}$ spin, and each HFS state is further split into finer doublet (SHFS) "hyperfine splitting" caused by the coupling of the $\bar{p}$ spin (S_p):

$$\boldsymbol{J} = \boldsymbol{F} + \boldsymbol{S_p}, \tag{10}$$
$$J_{-+} = F_- + 1/2 = L, \tag{11}$$
$$J_{--} = F_- - 1/2 = L - 1, \tag{12}$$
$$J_{++} = F_+ + 1/2 = L + 1, \tag{13}$$
$$J_{+-} = F_+ - 1/2 = L. \tag{14}$$

These quadruplet states lie from higher to lower energy, as shown in Fig. 11.

The hyperfine interaction is effectively expressed by

$$\begin{aligned}\mathcal{H}_{SHF} = {} & E_1(\boldsymbol{L}\cdot\boldsymbol{S_e}) + E_2(\boldsymbol{L}\cdot\boldsymbol{S_p}) + E_3(\boldsymbol{S_e}\cdot\boldsymbol{S_p}) \\ & + E_4\Big\{2L(L+1)(\boldsymbol{S_e}\cdot\boldsymbol{S_p}) - 6\big[(\boldsymbol{L}\cdot\boldsymbol{S_e})(\boldsymbol{L}\cdot\boldsymbol{S_p})\big]\Big\}\,.\end{aligned} \tag{15}$$

The 1st term, the $S_e - L_{\overline{p}}$ interaction, gives a dominant HF contribution. The 2nd, 3rd and 4th terms cause finer SHF level splitting within each member of HFS. The coefficients E_1, E_2, E_3 and E_4 are calculated by Bakalov and Korobov [33]. It is interesting to see how these individual terms behave. The 2nd term is the $\bar{\mathrm{p}}$ spin-orbit interaction, making the spin-up partners (J_{++} and J_{-+}) higher

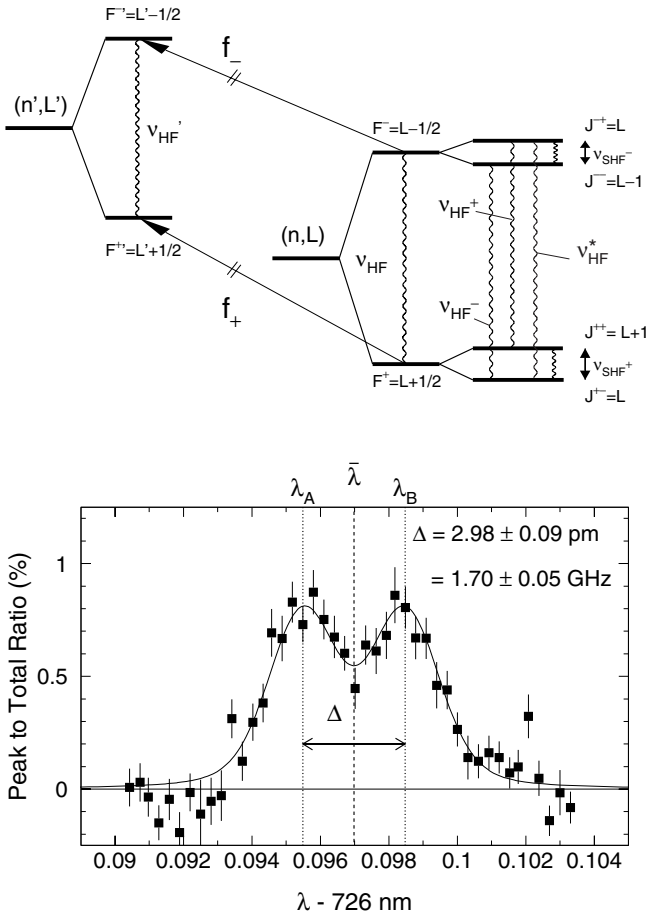

Fig. 11. (Upper) Splitting of $\bar{\mathrm{p}}\mathrm{He}^+$ states due to magnetic interactions, and observable laser transitions between the F^+ and F^- states according to Bakalov and Korobov [33]. (Lower) Observed hyperfine splitting of the unfavoured laser transition $(n, L) = (38, 34) \rightarrow (37, 35)$ [16]. The laser bandwidth is 1.2 GHz. The solid line is the result of a fit of two Voigt functions (a Gaussian fixed to the laser bandwidth convoluted with a Lorentzian to describe the intrinsic line width) to the spectrum. The intrinsic width of each lines was found to 0.4 ± 0.1 GHz. From Widmann *et al.* [16]

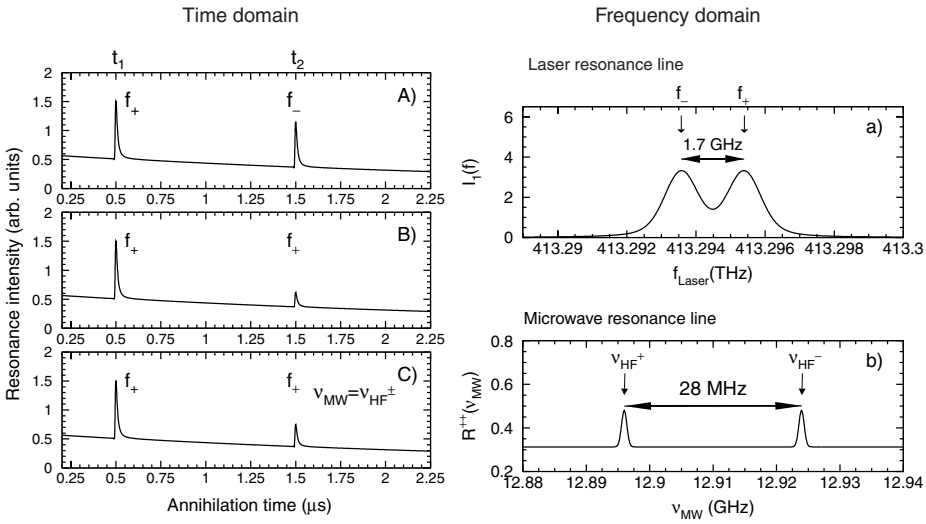

Fig. 12. Expected timespectra with laser spikes (left) and laser as well as microwave resonance curves (right)

lying than the spin-down partners (J_{+-} and J_{--}), respectively. The 3rd term is the e^--spin-$\bar{p}$-spin interaction, corresponding to the singlet-triplet separation as in the hydrogen case (except for the sign). This interaction favours the spin-triplet pairs ($\boldsymbol{S_p}$ parallel to $\boldsymbol{S_e}$) and thus, for F_+ the J_{++} member lies lower than the J_{+-} member, and for F_- the J_{--} member lies lower than the J_{-+} member, just opposite to the effect of the spin-orbit term. However, the 4th term, tensor term of the spin-spin interaction, bring a totally opposite level ordering, which cancel out the spin-spin contribution (3rd term). Then, the sum of all these terms looks as if only the spin-orbit interaction (2nd term) were responsible for SHFS.

The dominant resonance transitions are

$$L\,F_+J_{++} \leftrightarrow L\,F_-J_{+-}\ , \tag{16}$$

$$L\,F_+J_{-+} \leftrightarrow L\,F_-J_{--} \tag{17}$$

with different frequencies (ν^+_{HF} and ν^-_{HF}, respectively) in the microwave range (~ 13 GHz for the (37,35) state, see Fig. 11).

A method to observe microwave resonances in antiprotonic helium has been proposed and is being prepared for the coming antiproton decelerator (AD) ring at CERN [36]. It is called 2-laser-microwave triple resonance method, which has the following steps.

(i) Induce a population asymmetry of the hyperfine states (F_+ and F_-) by using the first laser tuned to one of the laser resonance double,
(ii) induce microwave resonance, and

(iii) detect the asymmetry inversion by the second laser.

The principle is shown in Fig. 12.

8 The Future

A new antiproton facility AD (antiproton decelerator) has been completed at CERN and a series of experimental programs are in progress. These include more systematic studies of the structure and formation of $\bar{p}He^+$, higher precision laser spectroscopy, microwave spectroscopy [36] and search for type-II antiprotonic helium based on the excited helium [37].

The author would like to thank his colleagues of the PS205 group of LEAR at CERN and also Drs. V.I. Korobov, D. Bakalov and G. Korenman for the helpful theoretical discussions. The present work is supported by the Grant-in-Aid for Creative Basic Research (10NP0101) of Monbusho of Japan.

References

1. M. Iwasaki *et al.*: Phys. Rev. Lett. **67**, 1246 (1991)
2. T. Yamazaki *et al.*: Nature **361**, 238 (1993)
3. G.T. Condo: Phys. Lett. **9**, 65 (1964)
4. J.E. Russell: Phys. Rev. Lett. **23**, 63 (1969); Phys. Rev. 188, 187 (1969)
5. T. Yamazaki and K. Ohtsuki: Phys. Rev. A **45**, 7782 (1992)
6. I. Shimamura: Phys. Rev. A **46**, 3776 (1992)
7. V.I. Korobov: Phys. Rev. A **54**, R1749 (1996)
8. Y. Kino, M. Kamimura and H. Kudo: Nucl. Phys. A **631**, 649c (1998)
9. N. Elander and E. Yarevsky: Phys. Rev. A **56**, 1855 (1997); A **58**, 2256(E) (1998)
10. N. Morita, K. Ohtsuki and T. Yamazaki: Nucl. Instr. Meth. A **330**, 439 (1993)
11. N. Morita *et al.*: Phys. Rev. Lett. **72**, 1180 (1994)
12. R.S. Hayano *et al.*: Phys. Rev. Lett. **73**, 1485 (1994)
13. F. Maas *et al.*: Phys. Rev. A **52**, 4266 (1995)
14. G. Ya. Korenman: Hyperfine Interactions **101/102**, 81 (1996), *ibid.*, 463
15. T. Yamazaki *et al.*: Phys. Rev. A **55**, R3295 (1997)
16. E. Widmann *et al.*: Phys. Lett. B **404**, 15 (1997)
17. V.I. Korobov and D. Bakalov: Phys. Rev. Lett. **79**, 3379 (1997)
18. H.A. Torii *et al.*: Phys. Rev. A **59**, 223 (1998)
19. V.I. Korobov: Hyperfine Interactions **119**, 185 (1999)
20. Y. Kino, M. Kamimura and H. Kudo: Hyperfine Interactions **119**, 201 (1999)
21. V.I. Korobov: *this edition*, pp. 517–520
22. G. Gabrielse *et al.*: Phys. Rev. Lett. **82**, 3198 (1999)
23. R. Hughes and B.I. Deutsch: Phys. Rev. Lett. **69**, 578 (1992)
24. E. Widmann *et al.*: Phys. Rev. A **51**, 2870 (1995)
25. E. Widmann *et al.*: Phys. Rev. A **53**, 3129 (1996)
26. M. Hori *et al.*: Phys. Rev. A **57**, 1698 (1998)
27. V.I. Korobov and I. Shimamura: Phys. Rev. A **56**, 4587 (1997)
28. D. Bakalov, B. Jeziorski, T. Korona, K. Szalewicz and E. Tchaukova: Phys. Rev. Lett. **84**, 2350 (2000)

29. T. Yamazaki *et al.*: Chem. Phys. Lett. **265**, 137 (1997)
30. R. Pohl *et al.*: Phys. Rev. A **58**, 4406 (1998)
31. B. Ketzer *et al.*: Phys. Rev. Lett. **78**, 1671 (1997)
32. B. Ketzer *et al.*: J. Chem. Phys. **109**, 424 (1998)
33. D. Bakalov and V.I. Korobov: Phys. Rev. A **57**, 1662 (1998)
34. H.A. Bethe and E.E. Salpeter: *Quantum mechanics of one- and two-electron atoms*, Springer, Berlin, 1957
35. A. Kreissl: Z. Phys. C **37**, 557 (1988)
36. T. Azuma *et al.*, Asacusa Experimental Proposal (1997), CERN/SPSC 97-19
37. O.I. Tolstikhin, S. Watanabe and M. Matsuzawa: Phys. Rev. A **54**, R3705 (1996)